

Estimation of Excited State Dipolemoments from Solvatochromic Shifts—Effect of pH

J. Jayabharathi · V. Kalaiarasi · V. Thanikachalam · K. Jayamoorthy

Received: 25 September 2013 / Accepted: 20 November 2013 / Published online: 9 January 2014
© Springer Science+Business Media New York 2014

Abstract Multicomponent, highly efficient, catalytic synthesis of some polysubstituted imidazole under solvent-free condition is reported. Characterization of polysubstituted imidazole have been carried out by X-ray diffraction (XRD) and spectral techniques. Electronic spectral studies reveal that their solvatochromic behavior depends not only on the polarity of the medium but also on the hydrogen bonding properties of the solvents. Specific hydrogen bonding interaction in polar solvents modulated the order of the two close lying lowest singlet states. The solvent effect on both the absorption and emission spectral results have been analyzed by multiple parametric regression analysis. Solvatochromic effects on the emission spectral position indicate the charge transfer (CT) character of the emitting singlet states both in a polar and a non polar environment. The fluorescence decays for the imidazole fit satisfactorily to a single exponential kinetics. The prototropic studies of N,N-dimethyl-4-(1,4,5-triphenyl-1H-imidazol-2-yl)naphthalen-1-amine (DTINA) reveal that two monocations [imidazole nitrogen protonated (MC1) and dimethylamino nitrogen protonated (MC2)] and a dication [both imidazole nitrogen and dimethylamino nitrogen protonated (DC)] are formed by protonation in both ground and excited states. These observations are in consistent with quantum chemical calculations.

Keywords Imidazole · Indium trifluoride · DFT · CT · HOMO-LUMO

J. Jayabharathi (✉) · V. Kalaiarasi · V. Thanikachalam · K. Jayamoorthy
Department of Chemistry, Annamalai University, Annamalaiagar, 608 002 Tamilnadu, India
e-mail: jtchalam2005@yahoo.co.in

Introduction

Polysubstituted imidazole derivatives have been used as highly sensitive fluorescent chemosensor for sensing, imaging metal ions and play an important role in material science due to their optoelectronic properties [1–4]. Its chelates with Ir^{3+} are major components for organic light emitting diodes [5]. Since they exert the properties of piezochromism, photochromism and thermochromism, they are used in molecular photonics [6]. Imidazole derivatives possess diverse biological activities, play important role as versatile building blocks for the synthesis of natural products [7–11]. Therefore, the synthesis of these imidazole derivatives has attracted much attention in organic synthesis.

The influence of solvents on fluorescence spectra and quantum yields may have several origins like perturbation, due to the solvent refractive index and dielectric constant to hydrogen bonding and complexation between the fluorophore and the solvent [12]. These factors can change the energy difference between the ground (S_0) and the first excited (S_1) states and can shift the emission or affect quantum yield. Solvent moderated shifts of the energy levels may enhance or inhibit radiationless transitions to the ground state via proximity effect [13].

In this work, naphthyl substituted imidazole derivatives are synthesized using indium trifluoride (InF_3) as a highly efficient catalyst. The spectral characteristics of the synthesised imidazole in solvents of different polarity, hydrogen bonding capacity and at different pH in aqueous media have been discussed. The Lippert solvent parameter Δf , the normalized $E_T(30)$ polarity scale, and the multiparameter Kamlet-Taft and Catalan solvent scales are used to describe the solvent effect on the fluorescence emission and stokes shift of imidazole derivatives. We have also addressed the influence of solvents on the photophysical properties of the synthesized molecules in terms of $hc\tilde{\nu}_{\text{abs}}^{\text{vac}}$, $hc\tilde{\nu}_{\text{flu}}^{\text{vac}}$ and $(hc\tilde{\nu}_{\text{abs}}^{\text{vac}} - hc\tilde{\nu}_{\text{flu}}^{\text{vac}})$ with solvent

polarity function. Our aim is also to investigate the effect of protic solvents on the fluorescence characteristics of DTINA and to understand the excited state prototropic equilibria of DTINA. Finally, the results obtained from the steady state and time resolved fluorescence studies have been rationalized with theoretical calculations.

Experimental

Spectral Measurements

The infrared spectra were recorded with an Avatar 330-Thermo Nicolet FT-IR spectrometer. The proton spectra at 400 MHz were obtained at room temperature using a Bruker 400 MHz NMR spectrometer. Proton decoupled ^{13}C NMR spectra were also recorded at room temperature employing a Bruker 400 MHz NMR spectrometer operating at 100 MHz. The mass spectra of the samples were obtained using a Thermo Fischer LC-Mass spectrometer in FAB mode. The cyclic voltammetry analyses were performed with CHI 630A potentiostap-electrochemical analyzer at a scan rate of 100 mV s^{-1} using 0.1 M tetra-(*n*-butyl)-ammonium hexafluorophosphate as supporting electrolyte with Ag/Ag^+ (0.01 M AgNO_3) as the reference electrode and Pt electrode as the working electrode under nitrogen atmosphere at room temperature.

The UV–vis absorption and fluorescence spectra were recorded with PerkinElmer Lambda 35 spectrophotometer and PerkinElmer LS55 spectrofluorimeter, respectively. Fluorescence lifetime measurements were carried out with a nanosecond time correlated single photon counting (TCSPC) spectrometer Horiba Fluorocube-01-NL lifetime system with NanoLED (pulsed diode excitation source) as the excitation source and TBX-PS as detector. The slit width was 8 nm and the laser excitation wavelength was 280 nm. The fluorescence decay was analyzed using DAS6 software. The quantum yield for all the imidazole were measured in dichloromethane using coumarin 47 in ethanol as the standard [14–16].

The radiative and non-radiative rate constants, k_r and k_{nr} , were deduced from the quantum yield (Φ_f) and lifetime (τ) using the equation, $\Phi_f = \Phi_{isc} \{k_r / (k_r + k_{nr})\}$; Φ_{isc} is the intersystem crossing yield, $k_r = \Phi_f / \tau$, $k_{nr} = 1 / (\tau) - \Phi_f / (\tau)$; $(\tau) = (k_r + k_{nr})^{-1}$. Single crystal XRD was recorded in Agilent Xcalibur Ruby Gemini diffractometer. The Radiation source is enhanced Mo X-ray source. Graphite monochromator used is of $10.5081\text{ pixels mm}^{-1}$ for the detector resolution.

Computational Details

The quantum chemical calculations were performed using the Gaussian-03 [17]. The geometry was fully optimized with the density functional theory (DFT) method, using B3LYP/6-31G (d,p) basis set. Computations of the vertical excitations,

difference density plots and optimization of the excited states were performed using time-dependent DFT (TD-DFT) using B3LYP/6-31G (d,p) basis set. The ground and excited states HOMO and LUMO frontier orbital's of imidazole derivatives were calculated by both DFT and TD-DFT methods at the B3LYP/ 6-31(d,p) level.

InF_3 -Catalyzed Facile and Rapid Synthesis of Polysubstituted Imidazole

A mixture of naphthaldehyde (1 mmol), benzil (1 mmol), aniline (1 mmol), ammonium acetate (1 mmol) and InF_3 (1 mol%) was stirred at solvent-free conditions at $80\text{ }^\circ\text{C}$, progress of the reaction was monitored by TLC. After completion of the reaction, the mixture was cooled, dissolved in acetone and filtered. The product was purified by column chromatography using benzene: ethyl acetate (9:1) as the eluent.

2-(naphthalen-1-yl)-4,5-diphenyl-1H-imidazole (1)

M.p. $258\text{ }^\circ\text{C}$., Anal. calcd. for $\text{C}_{25}\text{H}_{18}\text{N}_2$: C, 86.68; H, 5.24; N, 8.09. Found: C, 86.63; H, 5.21; N, 8.03. ^1H NMR (400 MHz, CDCl_3): δ 7.26–7.38 (m, 6H), 7.52–7.66 (m, 8H), 7.79 (d, Hz, 1H), 7.93 (bs, 2H), 7.98 (d, 1H), 8.82 (d, 1H), 10.41 (s, 10.4). ^{13}C NMR (100 MHz, CDCl_3): δ 125.11, 126.00, 126.37, 126.71, 127.20, 127.55, 127.88, 128.45, 128.69, 129.06, 129.75, 129.95, 134.93. MS: m/z. 346 [M^+].

2-(naphthalen-1-yl)-1, 4, 5-triphenyl-1H-imidazole (2)

M.p. $248\text{ }^\circ\text{C}$., Anal. calcd. for $\text{C}_{31}\text{H}_{22}\text{N}_2$: C, 88.12; H, 5.25; N, 6.63. Found: C, 88.08; H, 5.21; N, 6.60. ^1H NMR (400 MHz, CDCl_3): δ 6.88 (d, 2H), 7.03 (q, 3H), 7.22–7.31 (m, 10H) 7.47 (t, 2H), 7.66 (d, 2H), 7.80 (d, 2H), 8.19–8.20 (d, $J=5.6\text{ Hz}$, 1H). ^{13}C NMR (100 MHz, CDCl_3): δ 124.63, 126.04, 126.27, 126.63, 126.69, 127.53, 127.74, 127.84, 127.98, 128.10, 128.19, 128.31, 128.47, 128.61, 129.31, 129.42, 129.90, 130.81, 131.08, 132.83, 133.61, 134.57, 136.63, 138.10, 146.18. MS: m/z. 422 [M^+].

N,N-dimethyl-4-(1,4,5-triphenyl-1H-imidazol-2-yl)naphthalen-1-amine (3)

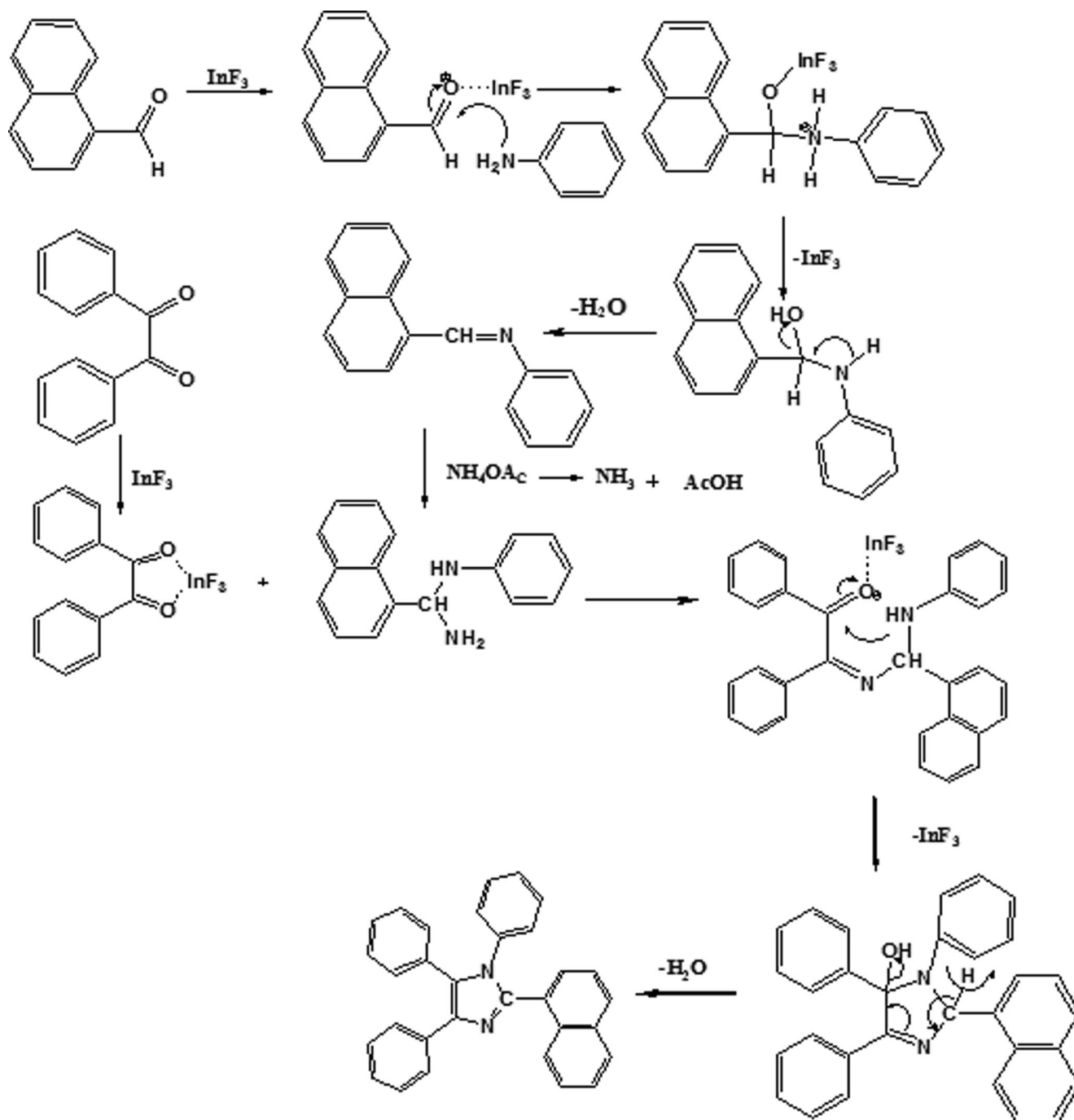
M.p. $261\text{ }^\circ\text{C}$., Anal. calcd. for $\text{C}_{33}\text{H}_{27}\text{N}_3$: C, 84.76; H, 6.25; N, 8.99. Found: C, 84.73; H, 6.23; N, 8.97. ^1H NMR (400 MHz, CDCl_3): δ 6.89 (d, 2H), 7.07 (q, 3H), 7.24–7.36 (m, 10H) 7.50 (t, 2H), 7.74 (d, 2H), 7.85 (d, 1H), 8.30 (d, 1H), 2.81 (s, 6H). ^{13}C NMR (100 MHz, CDCl_3): δ 124.83, 126.24, 126.43, 126.83, 126.99, 127.83, 127.94, 127.99, 128.18, 128.30, 128.39, 128.41, 128.53, 128.74, 129.47, 129.62, 129.94, 130.91, 131.48, 132.93, 133.71, 134.77, 136.83, 138.70, 146.98. MS: m/z. 465 [M^+].

Result and Discussion

Catalytic Activity of Indium Trifluoride

Initially, we have carried out the condensation reaction in the presence of an optimized molar ratio of InF_3 (1 mol%), naphthaldehyde (1 mmol), ammonium acetate (1 mmol), and arylamine (1 mmol) in different solvents such as water, ethanol, methanol, chloroform, and acetonitrile under refluxing and also in solvent-free conditions at 80 °C (Scheme 1). From these

experiments, it was clearly demonstrated that the solvent-free condition is the best for imidazole synthesis. In the absence of catalyst under solvent-free conditions at room temperature the yield is very poor even after 24 h. To enhance the yield of the desired product, the temperature of the reaction was increased to 200 °C, but no appreciable increment in the product yield was observed. We found that presence of a catalytic amount of InF_3 under solvent-free condition is the best for this synthesis; maximum yield (82 %) was obtained at 30 min on loading with 1 mol% of InF_3 at 80 °C (Table 1). Moreover, InF_3 can be



Scheme 1 Possible mechanism for InF_3 catalytic synthesis of imidazoles

Table 1 Effect of catalyst and temperature in the synthesis of imidazole derivatives

Entry	Temp (°C)	Solvent	InF ₃		InF ₃ (mol%)
			Time (min)	Yield (%)	
1	r.t	Solvent-free	130 (380)	70(Trace)	0.1
2	50	Solvent-free	65(250)	72(22)	0.1
3	70	Solvent-free	30(70)	76(45)	0.1
5	90	Solvent-free	25(90)	80(53)	0.1
6	80	Solvent-free	30	82	1
7	80	Solvent-free	25	85	2
8	80	Solvent-free	45	88	10
9	80	Water	100	35	1
10	80	Ethanol	40	65	1
11	80	Methanol	50	70	1
12	80	Chloroform	140	42	1
13	80	Acetonitrile	95	62	1

values in the parentheses corresponds to absence of catalyst

recovered and reused several times without significant loss of activity. High product yields, shorter reaction time, low catalyst loading and easy work-up procedure, make this procedure quite simple and more convenient. Our methodology could be a valid contribution to the existing processes of imidazole synthesis.

XRD Characterization of 2-(naphthalen-1-yl)-1, 4, 5-triphenyl-1H-imidazole (**2**)

2-(Naphthalen-1-yl)-1, 4, 5-triphenyl-1H-imidazole is a triclinic crystal and crystallizes in the space group $P\bar{1}$ with cell dimensions $a=11.1280(2)$, $b=14.8250(3)$ Å, $c=14.8820(2)$ Å

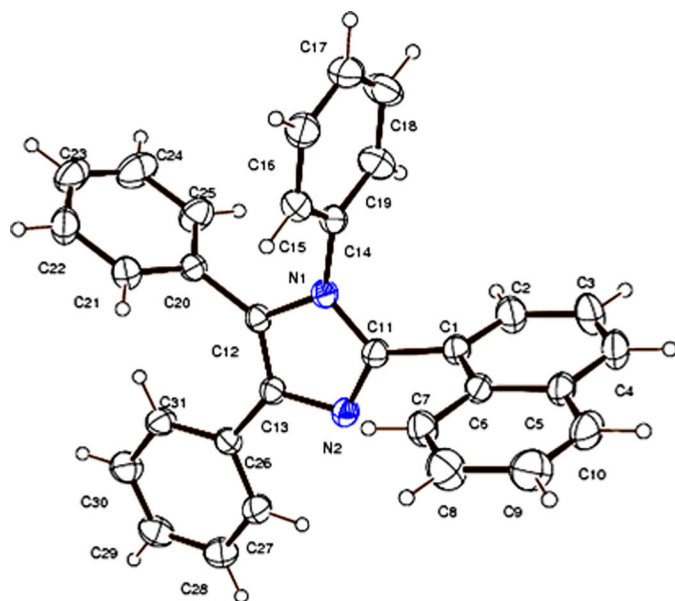


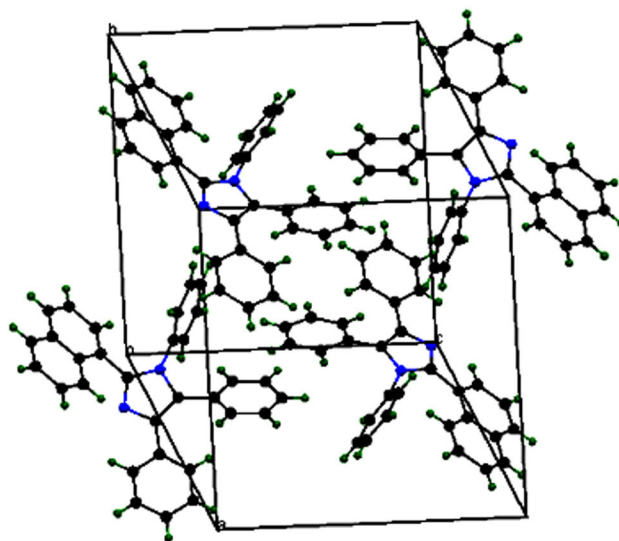
Fig. 1 ORTEP diagram of 2-(naphthalen-1-yl)-1, 4, 5-triphenyl-1H-imidazole

The ORTEP diagram is presented in Fig. 1. The imidazole unit is close to being planar [maximum deviation=0.59 (17) Å] and forms dihedral angles of 99.4.98° (2) and -101.0° (27) with the adjacent naphthyl and phenyl rings [C(2)-C(1)-C(11)-N(2)=99.4°(2), C(15)-C(14)-N(1)-C(11)=-101.0°(2)]. The dihedral angle between the latter two planes is -6.9° (3). In the crystal, molecules are consolidated into a three-dimensional architecture by π - π stacking interactions. Optimization of **2** has been performed by DFT at B3LYP/6-31G(d,p) level using Gaussian-03. All these XRD data are in good agreement with the theoretical values (Table S1). However, from the theoretical values it can be found that most of the optimized bond lengths, bond angles and dihedral angles are slightly higher than that of XRD values. These deviations can be attributed to the fact that the theoretical calculations are of isolated molecule in the gaseous phase and the XRD results are of the molecule in the solid state.

Solvent Modulated Absorption and Emission Behavior

Room temperature absorption and the fluorescence of imidazole derivatives (**1–3**) have been carried out. The absorption maxima of the studied compounds is shifted from 319 to 361 nm in solvents of varying polarity which corresponds to π - π^* transition of the molecule. The absorption is intense and the peak position is sensitive to the polarity of the medium. The magnitude of the shifts suggests that the ground state of the molecule is polar.

The emission spectra of **1–3** displayed in Fig. 2a, show a red-shifted band in the region of 335–452 nm from hexane to water. The fluorescence maximum is greatly affected by solvent polarity where a red-shifted fluorescence is observed on increasing



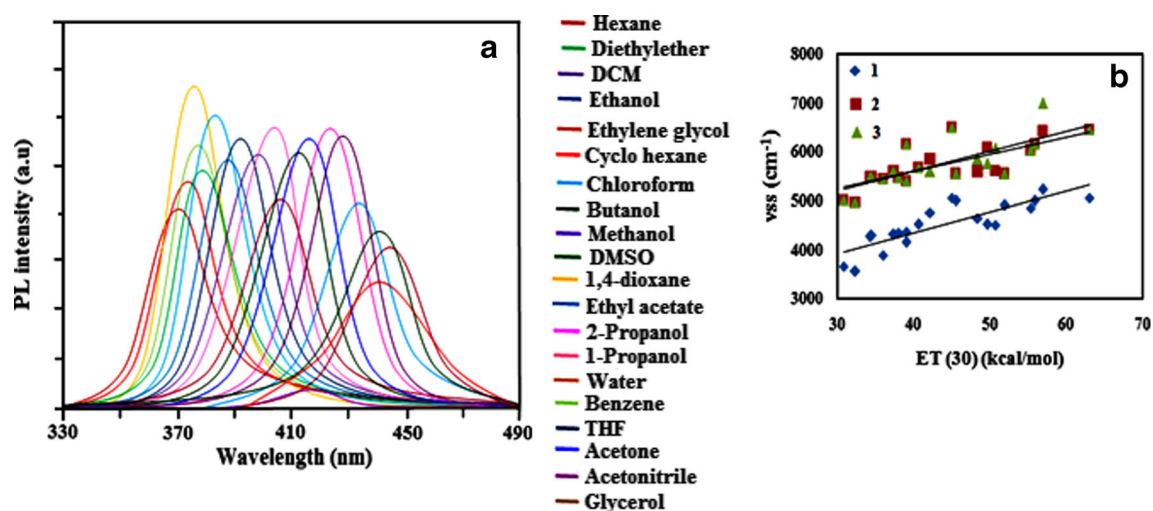


Fig. 2 a Emission profile of 3 in different solvents; b ν_{ss} cm⁻¹ Vs E_T(30)

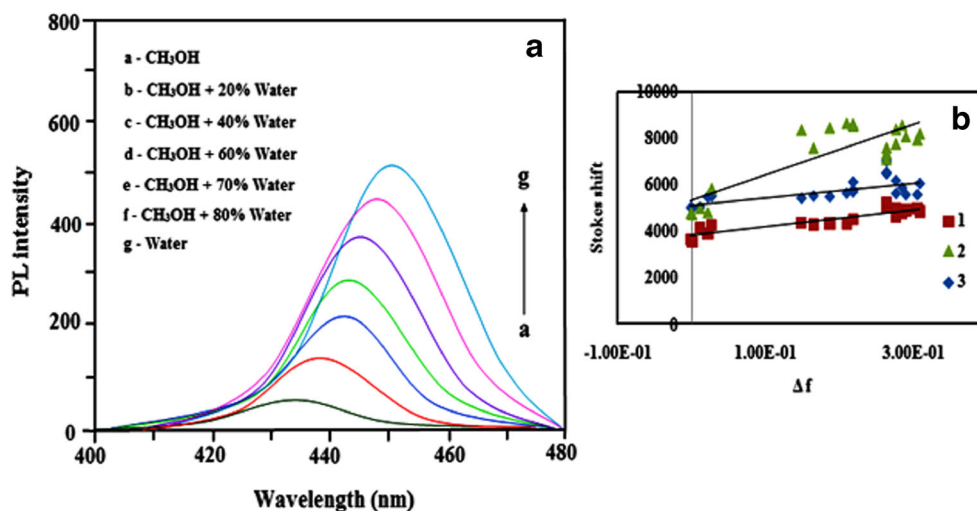
the solvent polarity. The effect of polarity of the medium on the fluorescence maximum is more intense than that on the absorption maximum. This observation suggests that the emitting state is more polar than the ground state [18–20]. The emission yields are more prominent in polar solvents compared to that of non-polar solvents. The linear variation of the Stokes shift with E_T(30) has been shown in Fig. 2b., where a double linear correlation is obtained [21]. Polar protic solvents fall on a separate line indicating that the mode of solvation of the emitting state is different from that in the other polar aprotic solvents. For polar protic solvents, gradual increment of Stokes shift is due to intermolecular hydrogen bonding interactions. The studied compounds exhibit overall increase of Stokes shift from non-polar to polar aprotic solvents mainly due to combined effect of increasing the polarity of the medium and intramolecular charge transfer (CT) state.

In order to obtain an insight about specific solvent–fluorophore interactions, the influence on fluorescence emission of 1–3 in methanol–water mixtures of different

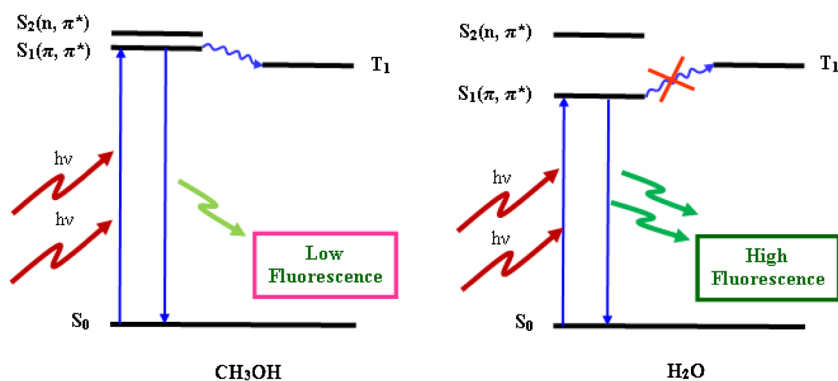
composition has been monitored and the spectra are illustrated in Fig. 3a. The addition of water to methanol–water mixture remarkably enhances the fluorescence of 1–3 with red shift. This effect may be described by the combined effect of hydrogen bonding and polarity of the medium. Mixing of two closely lying lowest singlet states (n, π^* and π, π^*) of imidazole derivatives favors the intersystem crossing [22]. As the polarity of the medium is increased, intermolecular hydrogen bonding interaction in the excited state stabilized the π, π^* state and enhancing the energy between the two states, which diminishes the mixing between the states (Scheme 2). As a result intersystem crossing from S₁ to T₁ decreases and an enhancement of fluorescence is observed.

The behavior of imidazole derivatives toward different solvent polarities may be interpreted in terms of the difference in the ground state and the excited state dipole moments. The spectral shift in fluorescence band may be attributed to the interaction between the dipole moment of the solute and the polarizability of the solvent. The extent of charge separation

Fig. 3 a Emission profile of 3 in MeOH as function of water composition; b Lippert–Mataga plot



Scheme 2 Schematic demonstration of modulation of the close-lying lowest singlet n , π^* and π , π^* states with solvent polarity in the excited state



on electronic excitation of **1–3** have been determined by measuring the change in the dipole moment ($\Delta\mu = \mu_e - \mu_g$) utilizing the spectral shift between the absorption and emission maxima as a function of solvent polarity. According to Lippert–Mataga equation [23] (1):

$$\bar{\nu}_{ss} = \bar{\nu}_{ab} - \bar{\nu}_{fl} = \text{const} + \left[\frac{2(\mu_e - \mu_g)^2}{hca^3} \right] f(D, n) \quad (1)$$

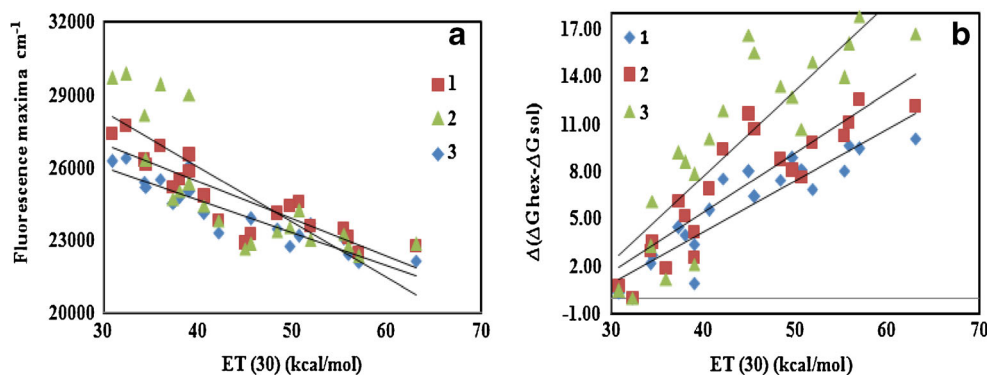
where $f(D, n) = (D-1)/(2D+1) - (n^2-1)/(2n^2+1)$, which indicates the orientation polarizability and depicts polarity parameter of the solvent, n is refractive index, D is dielectric constant, μ_e and μ_g are dipole moments of the species in S_1 and S_0 states, respectively, h is Planck's constant, c is velocity of light and a is Onsager's cavity radius. The Lippert–Mataga plot is linear for the non-polar and polar/aprotic solvents as shown in Fig. 3b; correlation is satisfactory. The geometrical optimization of **1–3** was done by DFT method using Gaussian-03 [17] to calculate the μ_g . Using μ_g value, 4.50D

Table 2 Adjusted coefficients ($(\nu_x)_0$, c_a , c_b and c_c) for the multilinear regression analysis of the absorption (ν_{ab}) and fluorescence (ν_{fl}) wavenumbers and Stokes Shift ($\Delta\nu_{ss}$) of imidazole derivatives (**1–3**)

with solvent polarity/polarizability, and acid and base capacity using the Taft (π^* , α and β) and the Catalan (SPP^N, SA and SB) scales

1	(ν_x)	(ν_x) ₀ cm ⁻¹	(π^*)	c_α	c_β
	λ_{ab}	$(3.04 \pm 0.03) \times 10^4$	$-(8.74 \pm 2.73) \times 10^3$	$(16.80 \pm 2.18) \times 10^3$	$-(100.82 \pm 16.56) \times 10^3$
	λ_{fl}	$(2.63 \pm 0.05) \times 10^4$	$-(11.73 \pm 1.52) \times 10^3$	$(21.92 \pm 1.94) \times 10^3$	$-(13.70 \pm 2.41) \times 10^3$
	$\Delta\nu_{ss} = \nu_{ab} - \nu_{fl}$	$(0.41 \pm 0.01) \times 10^4$	$(2.98 \pm 0.89) \times 10^3$	$-(5.12 \pm 0.19) \times 10^3$	$(2.88 \pm 0.11) \times 10^3$
	(ν_x)	(ν_x) ₀ cm ⁻¹	c_{SPP^N}	c_{SA}	c_{SB}
	λ_{ab}	$-(3.00 \pm 0.02) \times 10^4$	$-(7.98 \pm 1.66) \times 10^3$	$(12.11 \pm 2.79) \times 10^3$	$-(6.30 \pm 1.39) \times 10^3$
	λ_{fl}	$(2.57 \pm 0.03) \times 10^4$	$-(10.40 \pm 2.60) \times 10^3$	$(15.09 \pm 1.12) \times 10^3$	$-(7.68 \pm 1.89) \times 10^3$
	$\Delta\nu_{ss} = \nu_{ab} - \nu_{fl}$	$(0.42 \pm 0.01) \times 10^4$	$(2.41 \pm 0.03) \times 10^3$	$-(2.98 \pm 0.59) \times 10^3$	$(1.37 \pm 0.67) \times 10^3$
	(ν_x)	(ν_x) ₀ cm ⁻¹	(π^*)	c_α	c_β
	λ_{ab}	$(3.08 \pm 0.03) \times 10^4$	$-(10.14 \pm 1.62) \times 10^3$	$(24.33 \pm 3.70) \times 10^3$	$-(18.21 \pm 3.84) \times 10^3$
	λ_{fl}	$(2.53 \pm 0.04) \times 10^4$	$-(12.81 \pm 1.06) \times 10^3$	$(29.13 \pm 4.36) \times 10^3$	$-(20.88 \pm 3.83) \times 10^3$
	$\Delta\nu_{ss} = \nu_{ab} - \nu_{fl}$	$(0.54 \pm 0.02) \times 10^4$	$(2.67 \pm 0.55) \times 10^3$	$-(4.79 \pm 0.19) \times 10^3$	$(2.66 \pm 0.75) \times 10^3$
2	(ν_x)	(ν_x) ₀ cm ⁻¹	c_{SPP^N}	c_{SA}	c_{SB}
	λ_{ab}	$(3.05 \pm 0.02) \times 10^4$	$-(12.69 \pm 2.21) \times 10^3$	$(27.44 \pm 3.55) \times 10^3$	$-(16.31 \pm 3.58) \times 10^3$
	λ_{fl}	$(2.49 \pm 0.03) \times 10^4$	$-(13.97 \pm 2.62) \times 10^3$	$(27.43 \pm 3.43) \times 10^3$	$-(15.95 \pm 2.12) \times 10^3$
	$\Delta\nu_{ss} = \nu_{ab} - \nu_{fl}$	$(0.55 \pm 0.01) \times 10^4$	$(1.28 \pm 0.36) \times 10^3$	$(0.01 \pm 0.48) \times 10^3$	$-(0.35 \pm 0.25) \times 10^3$
3	(ν_x)	(ν_x) ₀ cm ⁻¹	(π^*)	c_α	c_β
	λ_{ab}	$(3.08 \pm 0.03) \times 10^4$	$-(8.44 \pm 2.52) \times 10^3$	$(18.51 \pm 3.36) \times 10^3$	$-(13.54 \pm 2.58) \times 10^3$
	λ_{fl}	$(2.54 \pm 0.04) \times 10^4$	$-(11.12 \pm 3.61) \times 10^3$	$(24.13 \pm 2.94) \times 10^3$	$-(17.29 \pm 3.72) \times 10^3$
	$\Delta\nu_{ss} = \nu_{ab} - \nu_{fl}$	$(0.54 \pm 0.01) \times 10^4$	$(2.68 \pm 1.42) \times 10^3$	$-(5.61 \pm 1.75) \times 10^3$	$(3.74 \pm 1.411) \times 10^3$
	(ν_x)	(ν_x) ₀ cm ⁻¹	c_{SPP^N}	c_{SA}	c_{SB}
	λ_{ab}	$(3.05 \pm 0.02) \times 10^4$	$-(10.30 \pm 3.62) \times 10^3$	$(18.72 \pm 3.95) \times 10^3$	$-(10.26 \pm 2.52) \times 10^3$
	λ_{fl}	$(2.50 \pm 0.02) \times 10^4$	$-(10.49 \pm 2.69) \times 10^3$	$(15.93 \pm 2.88) \times 10^3$	$-(8.23 \pm 1.45) \times 10^3$
	$\Delta\nu_{ss} = \nu_{ab} - \nu_{fl}$	$(0.55 \pm 0.01) \times 10^4$	$(0.18 \pm 0.02) \times 10^3$	$(2.79 \pm 0.11) \times 10^3$	$-(2.02 \pm 0.01) \times 10^3$

Fig. 4 **a** Fluorescence maxima and the $E_T(30)$; **b** $\Delta(\Delta G_{solv})$ Vs $E_T(30)$



(1), 4.3 D (2) and 5.0 D (3) obtained from the DFT calculation and the slope of Lippert–Mataga plot, the value of μ_c calculated is in the range, 6. 8–10 D for the studied imidazole.

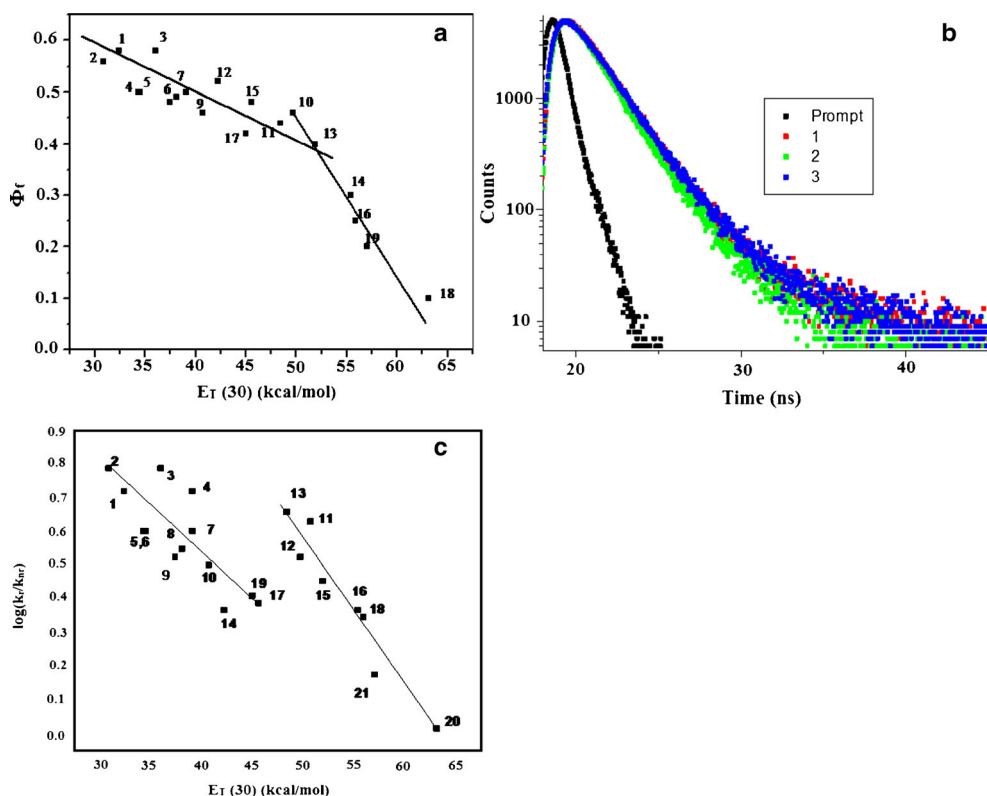
Multiple linear regression analysis is performed to identify the different modes of solvation determining the absorption and emission energies. Kamlet and Taft [24] put forward the π^* , α and β parameters to characterize the polarity/polarizability, the acidity and the basicity of a solvent respectively. Conversely, Catalan et al. [25] proposed an empirical solvent scales for polarity/polarizability (SPP), acidity (SA) and basicity (SB) to describe the respective properties of a given solvent

$$y = y_0 + a_\alpha \alpha + b_\beta \beta + c_{\pi^*} \pi^* \quad \text{(Kamlet–Taft)} \quad (2)$$

$$y = y_0 + a_{SA} SA + b_{SB} SB + c_{SPP} SPP \quad \text{(Catalan)} \quad (3)$$

The dominant coefficient affecting the absorption and fluorescence band of imidazole derivatives (1–3) are displayed in Table 2. Negative values of solvent dipolar interaction (π^*) and hydrogen bond accepting property (β) indicate these two parameters contribute to the stabilization of both the ground and the excited states of imidazole derivatives. The calculated ratio of β over π^* [1.24(ν_{abs}) & 1.17(ν_{emi}) (1), 1.60(ν_{abs}) & 1.55(ν_{emi}) (2) and 1.80 (ν_{abs}) & 1.63(ν_{emi}) (3)] reveal that interactions between imidazole derivatives and solvents with hydrogen bond accepting property (β) predominate in the excited state. A good linear variation is also obtained between the fluorescence maxima and $E_T(30)$ values [26] as shown by Fig. 4a. The free energy change of solvation and reorganization energies of 1–3 in various solvents have been estimated.

Fig. 5 **a** Quantum yield with $E_T(30)$; **b** Lifetime curves of 1–3 in ethanol; **c** $\log(k_r/k_{nr})$ Vs $E_T(30)$



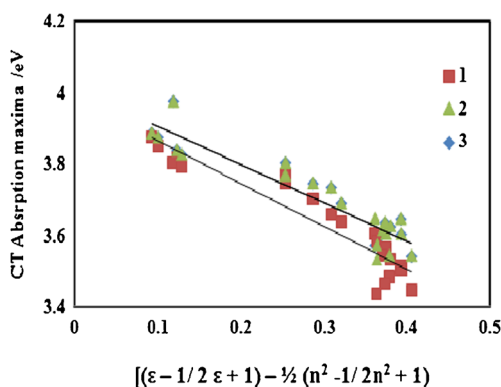


Fig. 6 CT Absorption maxima Vs solvent polarity function

According to Marcus [27], $E(A) = \Delta G_{\text{solv}} + \lambda_1$ and $E(F) = \Delta G_{\text{solv}} - \lambda_0$, where $E(A)$ and $E(F)$ are absorption and fluorescence band maxima in cm^{-1} , respectively, ΔG_{solv} is the difference in free energy of the ground and excited states in a given solvent and λ represents the reorganization energy. The free energy changes of solvation and reorganization energies of **1–3** in various solvents have been estimated. Under the condition that $\lambda_0 \approx \lambda_1 \approx \lambda$, we get, $E(A) + E(F) = 2\Delta G_{\text{solv}}$; $E(A) - E(F) = 2\lambda$. The ΔG_{solv} of **1–3** is maximum for hexane since it is purely non-polar and also α and β values of hexane are zero. The ΔG_{solv} is minimum in water. The difference between these values (water and hexane) should give the free energy change required for hydrogen bond formation. The plot of $\Delta(\Delta G_{\text{solv}}) = (\Delta G_{\text{hex}} - \Delta G_{\text{water}})$ versus $E_T(30)$ has been depicted in Fig. 4b. The difference in free energy of solvation in hexane and different hydrogen bonding solvents (i.e. ΔG_{solv}) of **1–3** follow the order of the hydrogen bond energy [28]. In the aprotic solvents the values are small and interaction of imidazole derivatives with those solvents is purely due to dipolar interactions in the excited state. The reorganization energy values of **1–3** have also been determined in different solvents. The definite values of reorganization energy confirmed the interaction between low frequency motions such as reorientation of solvent cell with low and medium frequency nuclear motion of the solute.

Table 3 Slopes and intercepts of the solvatochromic plots of the CT Fluorescence of the imidazoles (**1–3**)

Compound	Nonpolar solvents and Polar solvents		Polar solvents		Nonpolar solvents and Polar solvents	
	$hc\tilde{\nu}_{\text{abs}}^{\text{vac}}$, eV	$\frac{\mu_e(\mu_e - \mu_g)}{a_0^3}$	$hc\tilde{\nu}_{\text{abs}}^{\text{vac}}$, eV	$\frac{\mu_e(\mu_e - \mu_g)}{a_0^3}$	$\frac{\mu_e(\mu_e - \mu_g)}{a_0^3}$, eV	μ, D
1	3.48	1.13	3.61	1.23	1.407	6.00
2	3.56	1.35	3.93	1.45	1.509	6.65
3	3.38	1.66	3.63	1.86	1.023	8.09

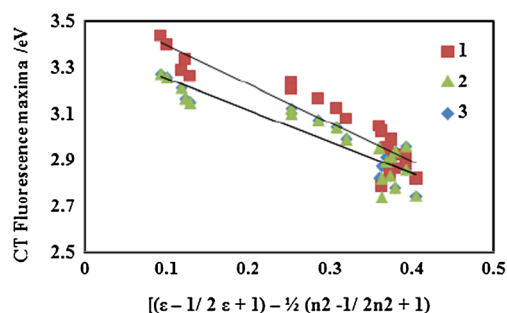


Fig. 7 CT Fluorescence maxima Vs solvent polarity function

Fluorescence quantum yield (ϕ_f) was measured in solvents of different polarity. The variation of ϕ_f with solvent polarity parameter $E_T(30)$ is depicted in Fig. 5a. A close look at the results shows that the ϕ_f values in various solvents are sensitive towards solvent polarity. The remarkable increase of ϕ_f in polar protic medium is compared with that in polar aprotic medium. This may be due to differential contribution of CT and hydrogen bonding interactions. Radiative (k_r) and nonradiative (k_{nr}) rate constants are calculated from fluorescence quantum yields and lifetime values (Fig. 5b) in different solvents to understand the effect of solvation on the dynamics of the excited state. The logarithm of (k_r/k_{nr}) is plotted against the solvent polarity parameter $E_T(30)$ which is shown in Fig. 5c. Two different straight lines are obtained, one for aprotic solvents and the other for protic solvents. In both the cases, upon increasing the polarity the logarithm ratio of radiative to nonradiative rate decreases but a steeper slope is obtained in the case of protic solvents. It indicates that the radiative and nonradiative rates are more sensitive toward protic solvents. It may be that the hydrogen bonding interaction in polar protic environment enhances the stabilization of the S_1 state as a result the nonradiative relaxation rate increases [29].

An interesting result is provided by the effect on the shift of the CT absorption bands with increasing solvent polarity (Fig. 6) [30, 31]. With the assumption that point dipole is at the center of the spherical cavity and the mean solute polarizability (α) to be insignificant, it follows,

$$hc\tilde{\nu}_{\text{abs}}^{\text{vac}} \approx hc\tilde{\nu}_{\text{abs}}^{\text{vac}} - 2 \mu_g(\mu_e - \mu_g) / \alpha_0^3 [(\epsilon - 1/2\epsilon + 1)^{-1} / 2(n^2 - 1/2n^2 + 1)] \quad (4)$$

where μ_g and μ_e are the dipole moments of the solute in the ground and excited state, correspondingly, ν_{abs} and $\tilde{\nu}_{\text{abs}}^{\text{vac}}$ are the spectral positions of a solvent-equilibrated absorption maxima and the value extrapolated to the gas-phase, respectively, a_0 is the effective radius of the Onsager cavity, [32] and ϵ and n are the static dielectric constant and the refractive index of the solvent, respectively. In the case of the well-separated CT absorption bands, Eq. 4 is used to determine the values of $\mu_g(\mu_e - \mu_g) / \alpha_0^3$ and $\tilde{\nu}_{\text{abs}}^{\text{vac}}$ and the values are displayed in Table 3. In the excited state,

Table 4 Frontier Orbital Energies along with dipole moment of **1–3** and MC1, MC2 and DC

Comd.	Dipole Moment μ_e/μ_g D	HOMO ev	LOMO ev	HOMO-1 ev	LOMO+1 ev	$E_{\text{HOMO}}-E_{\text{LUMO}}$ ev
1	4.5/8.8	-8.54(4.31)	-0.89(3.20)	-8.95	0.00	1.07(1.11)
2	4.3/7.9	-8.56(4.52)	-5.88(2.02)	-7.64	3.11	2.68(2.50)
3	5.0/9.9	-7.35(3.96)	2.39(1.01)	-7.62	3.10	4.96(2.95)
MC ₁	22.6	-9.22	-1.33	-10.34	-0.08	7.89
MC ₂	11.4	-10.18	-0.60	-11.13	-0.27	9.58
DC	20.6	-5.85	-5.23	-8.65	-5.08	0.62

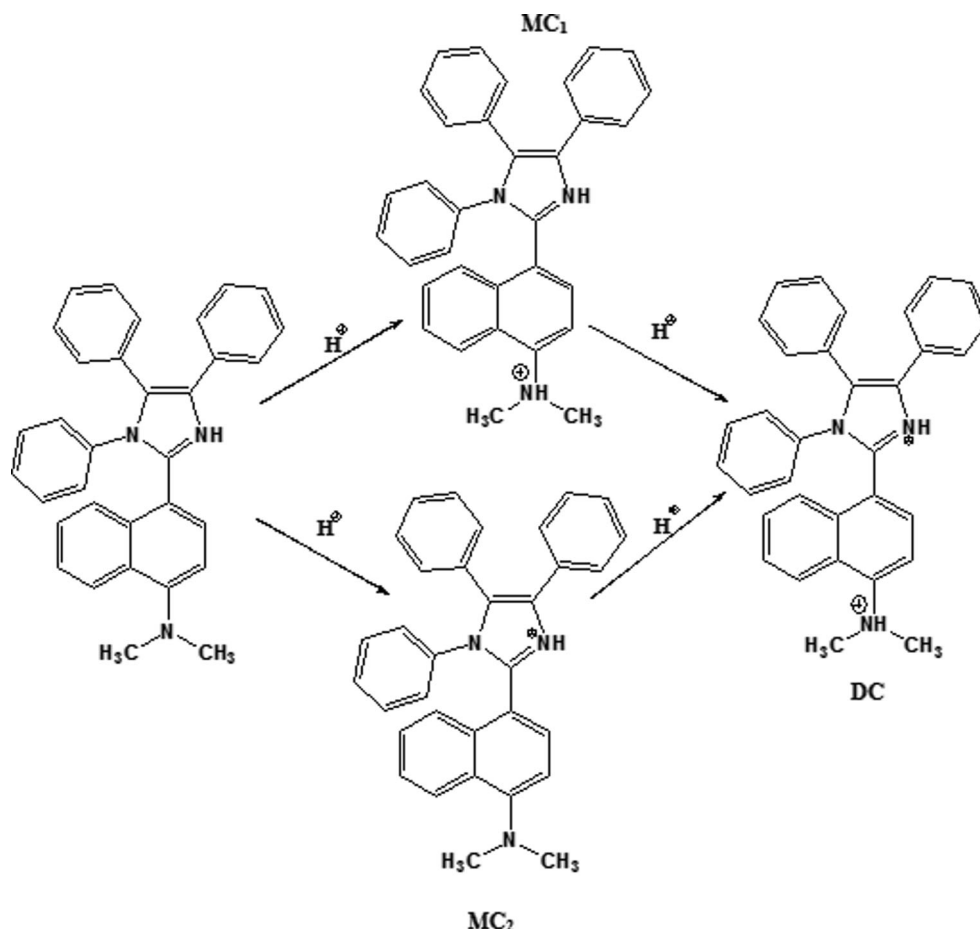
values in the parentheses are experimental

the negative and positive ends of the electric dipole are localized nearly in the centers of the donor and acceptor fragments respectively. A considerable shift of their spectral position and the increase of the Stokes shift and enlargement of the emission bandwidth with increasing solvent polarity in fluorescence spectra point to the CT character of the fluorescent states and clearly indicate that the absolute values of μ_e are much higher than those of μ_g . The excited state dipole moments μ_e can be estimated by the fluorescence solvatochromic shift method due to the fact that the excited states live sufficiently long with respect to the orientation relaxation time of the solvent [33–36].

Under the same assumptions as used for expression 4, it follows that

$$hc\tilde{\nu}_{\text{flu}} \approx hc\tilde{\nu}_{\text{flu}}^{\text{vac}} - 2\mu_e(\mu_e - \mu_g)/\alpha_0^3 [(\epsilon - 1/2\epsilon + 1)^{-1} / 2(n^2 - 1/2n^2 + 1)] \quad (5)$$

where $\tilde{\nu}_{\text{flu}}$ and $\tilde{\nu}_{\text{flu}}^{\text{vac}}$ are the spectral positions of the solvent equilibrated fluorescence maxima and the value extrapolated to the gas-phase, respectively. The compounds studied show a satisfying linear correlation between the energy $hc\tilde{\nu}_{\text{flu}}$ and the solvent polarity function in a polar environment and also in all the solvents (Fig. 7) [37]. The values of $\mu_e(\mu_e - \mu_g)/\alpha_0^3$ are

Scheme 3 Possible mono and dictations

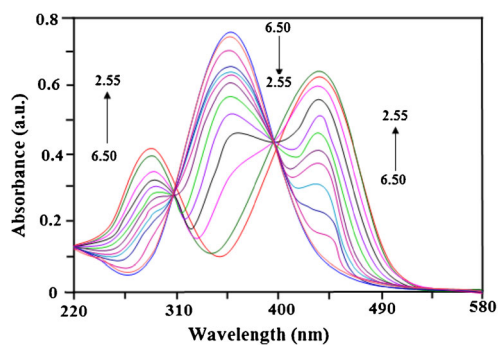


Fig. 8 Absorption spectra of **3** for neutral-monocation equilibrium

displayed in Table 3. The values extracted from the data measured in polar media are somewhat larger than those resulting from the analysis of the data obtained for the whole range of the solvents. This finding can be explained only by the dependence of the electronic structure of the fluorescent states on solvation. Due to a relatively small energy gap between the lowest internal charge transfer (ICT) states and the states excited locally in the nonpolar solvents, which leads to increase of

Table 5 Electronic Spectral data of **3** and their mono and dications along with cation abundance

Species	λ_{abs}	λ_{exci}	λ_{emi}
3	350	351	452
MC ₁	306	306	424
MC ₂	432	432	570
DC	317	317	436
pka	Cation abundance		
3.25	MC ₁ » MC ₂		
4.50	MC ₂ > MC ₁		
0.20	DC > MC		

the contribution of the (π , π^*) character to the wave function of the CT states. It leads to a lowering of energy with respect to a pure CT state because of a stabilizing character of such interactions and red shift obtained in the fluorescence spectra.

Under the assumption that the CT fluorescence corresponds to the state reached directly upon excitation, the quantity $(\mu_e - \mu_g)/\alpha_0^3$ can be evaluated from the solvation effects on the Stokes shift,

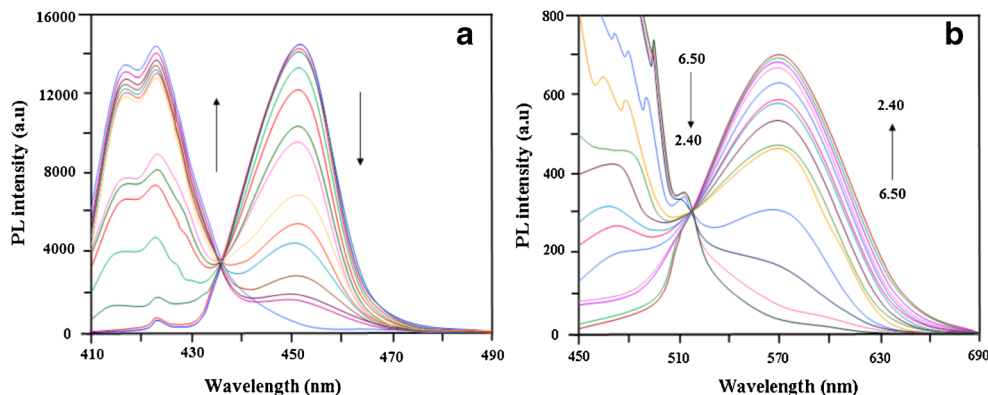
$$hc(\tilde{\nu}_{\text{abs}} - \tilde{\nu}_{\text{flu}}) = hc(hc\tilde{\nu}_{\text{abs}}^{\text{vac}} - hc\tilde{\nu}_{\text{flu}}^{\text{vac}}) + 2(\mu_e - \mu_g)^2/\alpha_0^3[(\epsilon - 1/2 \epsilon + 1)^{-1/2} (n^2 - 1/2n^2 + 1)] \quad (6)$$

The compounds studied show a satisfying linear correlation between the energy $hc\tilde{\nu}_{\text{abs}} - hc\tilde{\nu}_{\text{flu}}$ and the solvent polarity function in a polar environment and also in all the solvents studied; the values of $(\mu_e - \mu_g)/\alpha_0^3$ are 1.407 eV (**1**), 1.509 eV (**2**), and 1.023 eV (**3**). The Eqs. 4–6 relate the measured quantities to the excited state dipole moments μ_e . Under the assumption that $\mu_e \gg \mu_g$ and with the effective spherical radius of the molecules a_0 , 5.21 Å (**1**), 5.27 Å (**2**), and 5.29 Å (**3**), as estimated from the molecular dimensions of the compounds calculated by molecular mechanics, Eqs. 5 and 6 yield very

similar values of μ_e being in the range of 6.00 D (**1**), 6.65 D (**2**) and 8.09 D (**6**) for the studied molecules.

The electrochemical properties of the imidazole (**1–3**) have been examined by cyclic voltammetry and the redox potentials have been measured from the plot potential *versus* current. The energies of the highest occupied molecular orbital (HOMO) and lowest unoccupied molecular orbital (LUMO) have been calculated using the relation, $E_{\text{HOMO}} = 4.8 + E_{1/2}^{\text{oxi}}$; $E_{\text{LUMO}} = E_{\text{HOMO}} - 1239/\lambda_{\text{onset}}$ and the calculated values are given in Table 4. The LUMO

Fig. 9 **a** Emission spectrum of **3** at excitation 336 nm **b** Emission spectrum of **3** at excitation 432 nm



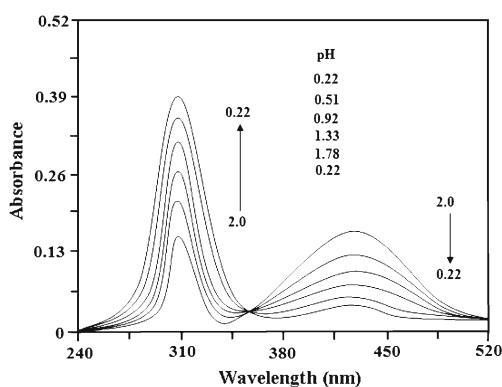


Fig. 10 Absorption spectra of **3** for monocation-dication equilibrium

energies have been deduced from the HOMO energies and the lowest-energy absorption edges of the UV–vis absorption spectra. The calculated energy gap ($E_g = E_{\text{HOMO}} - E_{\text{LUMO}}$) of **1–3** are 1.11, 2.50 and 2.95 eV. Therefore, the HOMO stability and the emission energy gap are controlled by the nature and substituent present in the imidazole moiety.

Prototropic Equilibria

Upon protonation of the basic nitrogens in DTINA, the formed possible mono and dication species are presented in Scheme 3. Decreasing the pH two new peaks at 306 and 432 nm appear in the absorption spectra with two isobestic points at 336 nm and 397 nm. Figure 8, presents the absorption spectra. This indicates the formation of two types of monocations. Excitation at 336 nm resulted two emission peaks at 424 and 452 nm with an isoemissive point at 434 nm which confirmed the equilibrium between the neutral form and the monocation (Fig. 9a). The

emission peak at 452 nm corresponding to the neutral molecule is predominantly observed when excited at 397 nm. The intensity of the neutral fluorescence band decreases with increase in acid concentration. Excitation at 432 nm produces an additional emission at 570 nm which is shown in Fig. 9b. Decreasing the pH increases the intensity of the emission at 570 nm. All these interesting results are displayed in Table 5 and confirmed two types of monocations are formed in both ground and excited states. Protonation of the dimethylamino nitrogen leads to a blue shift and protonation of the imidazole nitrogen leads to a red shift [38–40]. In DTINA, due to an increase in charge flow from the dimethylamino nitrogen to the imidazole nitrogen, protonation predominantly occurs at the imidazole nitrogen and a small amount of protonation occurs at the dimethylamino nitrogen [41]. Therefore the blue shifted band at 306 nm in the absorption maximum and the corresponding fluorescence maximum at 424 nm can be assigned to the monocation formed by the protonation of dimethylamino nitrogen, i.e. MC1 (Scheme 3) whereas the red-shifted absorption and the fluorescence spectra are assigned to the monocation formed by the protonation of the imidazole nitrogen (MC2). Decreasing the pH of a solution below 2 causes a decrease in the absorbance of MC1 and the absorption spectrum of MC2 also undergoes a bathochromic shift with an increase in absorbance as displayed in Fig. 10. At pH 0.20, absorption peak is observed at 317 nm and the emission band at 360 nm can be assigned to DC. These changes are consistent with a shift of the equilibrium towards the dication from the monocation. As expected it is red shifted with respect to MC1 and blue shifted compared to MC2.

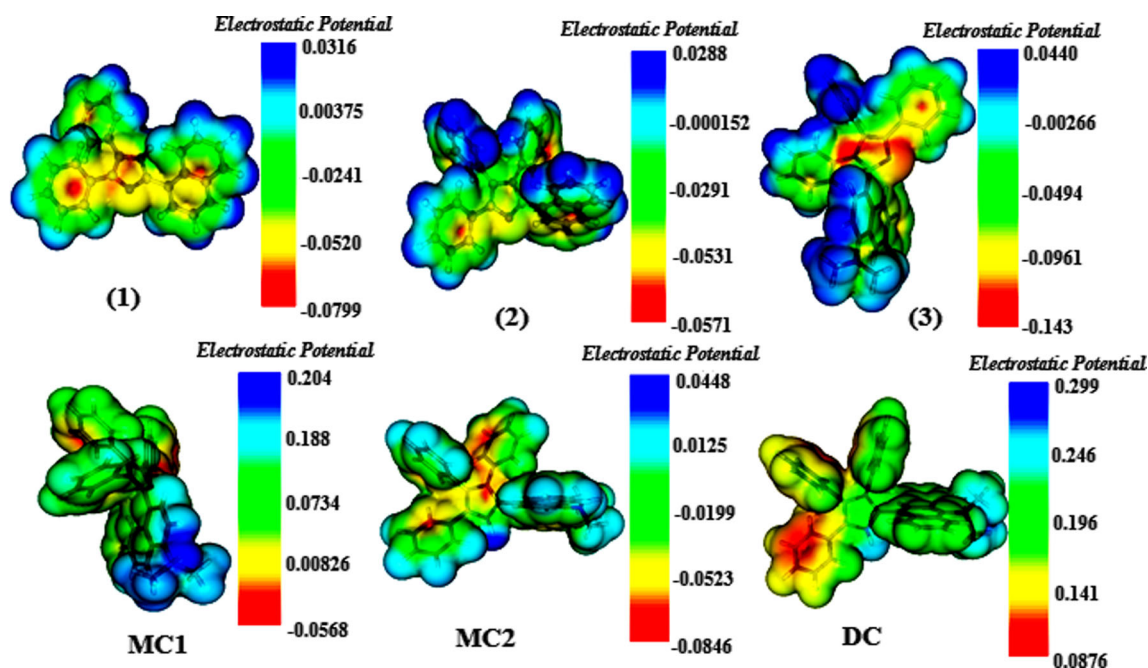


Fig. 11 MEP diagram

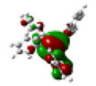
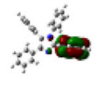
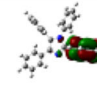
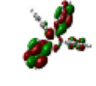
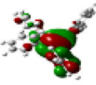
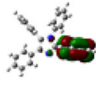
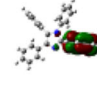
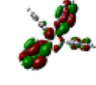
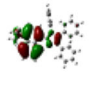
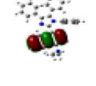

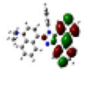
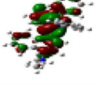
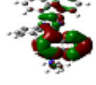
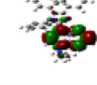
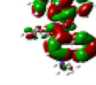
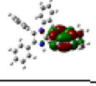
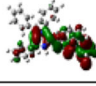
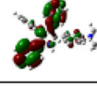
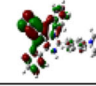
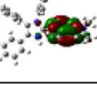
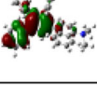
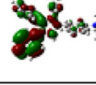
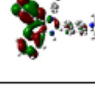
COMP.D.	HOMO	HOMO -1	LUMO	LUMO+1
1				
2				
3				
MC ₁				
MC ₂				
DC				

Fig. 12 HOMO-LUMO contour maps calculated by DFT/B3LYP/6-31G(d,p)

Protonation Vs Computational Studies

In order to supplement the experimental predominant site of protonation, the charge distribution was calculated by the natural bond orbital (NBO) and Mulliken methods [DFT/B3LYP/6-31G (d,p)]. These two methods predict the same tendencies. The calculated charges for imidazole nitrogen ($-\text{N}=\text{N}$) [$-0.57(\mathbf{1})$; $-0.61(\mathbf{2})$; $-0.73(\mathbf{3})$] and for dimethylamino nitrogen ($-\text{NMe}_2$) [$-0.55(\mathbf{3})$]. The charge distribution shows that the more negative charge is concentrated on imidazole nitrogen atom whereas the partial positive charge resides at hydrogens. Among the imidazole and dimethylamino nitrogen atoms, imidazole nitrogen atom is considered as more basic site

The higher electron density at the nitrogen atoms ($-\text{N}=\text{N}$) in imidazole was also supported by molecular electrostatic potential (MEP) which is shown in Fig. 11. The MEP map clearly suggests that nitrogen atoms represent the most negative potential region (dark red) The hydrogen atom attached to the six membered ring bear the maximum positive charge (blue region). The predominance of green region in the MEP surface corresponds to a potential halfway between the two extremes red and dark blue color. In compound **3** the imidazole nitrogen atom seems to exert comparatively more negative potential as compared to dimethylamino nitrogen atom. The MEP clearly confirms the existence of the electrophilic active center nitrogens characterized by red color.

Further the electron density distribution has been studied using the frontier molecular orbitals by DFT analysis. The 3D plots of the frontier orbitals HOMO and LUMO for the imidazole **1–3** are shown in Fig. 12. The HOMO orbital acts as an electron donor and the LUMO orbital acts as an acceptor.

In compound **1**, the HOMO is located on the imidazole ring, both phenyl rings at C12, C13 carbon atoms of the imidazole ring and partly on the naphthyl ring at C11 carbon whereas the LUMO is located partly on the phenyl rings at C12, C13 carbon atoms and partly on the naphthyl ring at C11 carbon. In compound **2**, while the HOMO is on the imidazole ring and partly on the phenyl ring at N1, the LUMO is located only on the phenyl ring at C11 of the imidazole ring. For **3**, the HOMO is on the imidazole ring and on the N,N-dimethylaminonaphthyl ring at C11 carbon and the LUMO is imidazole ring and on the phenyl rings at C12, C13 carbon atoms of the imidazole ring. The electron density analysis on the HOMO-LUMO orbital supports the flow of electron from dimethylamino group to imidazole nitrogen. The HOMO \rightarrow LUMO transition implies that intramolecular charge transfer takes place within the molecule. The energy gap (E_g) of imidazole has been calculated from the HOMO and LUMO energy levels. The energy gap explains the probable charge transfer (CD) inside the chromophores.

In MC₁, HOMO is located on the entire molecule whereas LUMO is partly on the naphthyl ring at C11 carbon and on imidazole ring. For MC₂ and DC, HOMO is located partly on the naphthyl ring at C11 carbon and LUMO is partly on imidazole ring, phenyl ring at N1 and both phenyl rings at C12, C13 carbon atoms of the imidazole ring.

Conclusion

In this work, we found a thermal exposure synthetic method for polysubstituted imidazole that is simple, efficient and green via a

multicomponent one-pot reaction in the presence of InF_3 as an inexpensive and eco-friendly catalyst in solvent-free conditions. Photophysical studies reveal that the solvatochromic behavior of imidazole derivatives depend not only the polarity of the medium but also the hydrogen bonding properties of the solvents. The quantum yield decreases in polar protic solvents due to an increase in the nonradiative rate by hydrogen bonding interactions. Kamlet–Taft analysis shows that in the excited state, imidazole derivatives form a stable complex with solvents with high hydrogen bond acceptance abilities and low hydrogen bond donor character. The compounds studied show a satisfying linear correlation between the energy $hc\tilde{\nu}_{\text{abs}}$, $hc\tilde{\nu}_{\text{flu}}$, $hc\tilde{\nu}_{\text{abs}}-hc\tilde{\nu}_{\text{flu}}$ and the solvent polarity function in a polar environment. Hydrogen bonding interaction in protic polar environment enhances the stabilization of S_1 state which leads to reduce the mixing between the states and as a result decrease of non-radiative relaxation is observed. The theoretical results based on density functional theory are in good agreement with experimental data.

References

- Lefebvre JF, Leclercq D, Gisselbrecht JP, Richeter S (2010) *Eur J Org Chem* 1912–1920
- Shi L, Su J, Wu Z (2011) *Inorg Chem* 50:5477–5484
- Adachi M, Nagao M (2001) Design of near-infrared dyes based on pi-conjugation system extension 2. Theoretical elucidation of framework extended derivatives of perylene chromophore. *Chem Mater* 13:662–669
- Hung WS, Lin JT, Chien CH, Tao YT, Sun SS, Wen YS (2004) Highly phosphorescent Bis-Cyclometalated iridium complexes containing Benzoimidazole-based ligands. *Chem Mater* 16:2480–2488
- Chen CH, Shi J (1998) Review as emitting material for electroluminescence. *Coord Chem Rev* 171:161–174
- Fridman N, Kaftory M, Speiser S (2007) Structures and photophysics of lophine and double lophine derivatives. *Sensors Actuators B* 126:107–115
- Golan DE, Armstrong AW (2007) Principles of pharmacology: The pathophysiologic basis of drug therapy, Wolters Kluwer Health
- Bhat NR, Zhang PS, Mohanty SB (2007) MAP kinase regulation of oligodendrocyte differentiation with CREB as a potential target. *Neurochem Res* 32:293–302, p38
- Lombardino JG, Wiseman EH (1974) Preparation and antiinflammatory activity of some nonacidic trisubstituted imidazole. *J Med Chem* 17:1182–1188
- Misono M (2001) Unique acid catalysis of heteropoly compounds (heteropolyoxometalates) in the solid state. *Chemical Communications* 1141–1152
- Chang LL, Sidler KL, Cascieri MA, de Laszlo S, Koch G, Li B, MacCoss M, Mantlo N, Okeefe S, Pang M, Rolando A, Hagmann WK (2001) *Bioorganic and Medicinal Chemistry Letters* 11:2549–2553
- Lakowicz JR (2006) Principles of fluorescence spectroscopy, 3rd edn. Springer, New York
- Lim EC (1986) *J Phys Chem* 90:6770
- Jayabharathi J, Thanikachalam V, Jayamoorthy K, Srinivasan N (2013) Synthesis, spectral studies and solvatochromism of some novel imidazole derivatives—ESIPT process. *Spectrochim. Acta Part A* 105:223–228
- Jayabharathi J, Thanikachalam V, Sathishkumar R, Jayamoorthy K (2012) *Photochem Photobiol B*: 117:222–227
- Jayabharathi J, Thanikachalam V, Sathishkumar R, Jayamoorthy K (2013) *Spectrochim Acta Part A*: 101:249–253
- Frisch MJ, Trucks GW, Schlegel HB, Scuseria GE, Robb MA, Cheeseman JR, Montgomery JA Jr, Vreven T, Kudin KN, Burant JC, Millam JM, Iyengar SS, Tomasi J, Barone V, Mennucci B, Cossi M, Scalmani G, Rega N, Petersson GA, Nakatsuji H, Hada M, Ehara M, Toyota K, Fukuda R, Hasegawa J, Ishida M, Nakajima T, Honda Y, Kitao O, Nakai H, Klene M, Li X, Knox JE, Hratchian HP, Cross JB, Bakken V, Adamo C, Jaramillo J, Gomperts R, Stratmann RE, Yazyev O, Austin AJ, Cammi R, Pomelli C, Ochterski JW, Ayala PY, Morokuma K, Voth GA, Salvador P, Dannenberg JJ, Zakrzewski VG, Dapprich S, Daniels AD, Strain MC, Farkas O, Malick DK, Rabuck AD, Raghavachari K, Foresman JB, Ortiz JV, Cui Q, Baboul AG, Clifford S, Cioslowski J, Stefanov BB, Liu G, Liashenko A, Piskorz P, Komaromi I, Martin RL, Fox DJ, Keith T, Al-Laham MA, Peng CY, Nanayakkara A, Challacombe M, Gill PMW, Johnson B, Chen W, Wong MW, Gonzalez C, Pople JA (2004) *Gaussian 03 (Revision E.01)*. Gaussian, Inc, Wallingford
- Pramanik S, Banerjee P, Sarkar A, Mukherjee A, Mahalanabis KK, Bhattacharya SC (2008) *Spectrochim. Acta Part A: Mol Biomol Spec* 71:1327
- Willard DM, Riter RE, Levinger NE (1998) Dynamics of Polar Solvation in Lecithin/Water/Cyclohexane Reverse Micelles. *J Am Chem Soc* 120:4151–4160
- Saha S, Samanta A (2002) Influence of the structure of the amino group and polarity of the medium on the photophysical behavior of 4-amino-1,8-naphthalimide derivatives. *J Phys Chem A* 106:4763–4771
- Reichardt C (1988) Solvents and solvent effects in organic chemistry, 2nd edn. VCH, Weinheim
- de Melo JSS, Becker RS, Macanita AL (1994) *J Phys Chem* 98:6054–6058
- Lippert E (1957) Spektroskopische bestimmung des dipolmomentes aromatischer verbindungen im ersten angeregten singulettzustand. *Z Electrochem* 61:962–975
- Kamlet MJ, Taft RW (1976) The solvatochromic comparison method. 1. The scale of solvent hydrogen-bond acceptor (HBA) basicities. *J Am Chem Soc* 98:377–383
- Catalan J, Lopez V, Perez P (1996) Use of the SPP scale for the analysis molecular system with dual emissions resulting from the solvent polarity. *J Fluoresc* 6:15–22
- Reichardt C (1979) Empirical parameters of solvent polarity as linear free energy elationships. *Angew Chem Int Ed Engl* 18:98–110
- Marcus RA (1963) Free energy of non equilibrium polarization systems. II. Homogeneous and electrode systems. *J Chem Phys* 38:1858
- Castellan GW (1985) *Physical chemistry*, 3rd edn. Narosa Publishing House, Delhi
- Dhar S, Rana DK, Roy SS, Roy S, Bhattacharya S, Bhattacharya SC (2012) Effect of solvent environment on the photophysics of a newly synthesized bioactive 7-oxy(5-selenocyanato-pentyl)-2H-1-benzopyran-2-one. *J Lumin* 132:957–964
- Rettig W, Zander M (1982) On twisted intramolecular charge transfer (TICT) stated in N-aryl-carbazoles. *Chem Phys Lett* 87:229–234
- Chiba K, Aihara JI, Araya K, Matsunaga Y (1980) *Bull Chem Soc Jpn* 53:1703
- Onsager L (1936) Electric moments of molecules in liquids. *J Am Chem Soc* 58:1486–1493
- Böttcher CJF (1973) In: Van Belle OC, Bordewijk P, Rip A (eds) *Theory of electric polarization*, vol I. Elsevier, Amsterdam
- Lippert EZ (1955) *Naturforsch A* 10:541
- Mataga N, Kaifu Y, Koizumi M (1955) The solvent effect on fluorescence spectrum. Change of solute-solvent interaction during the lifetime of excited solute molecule. *Bull Chem Soc Jpn* 28:690–691
- Liptay W (1974) In: Lim EC (ed) *Excited states*. Academic, New York, p 129
- McRae EG (1957) Theory of solvent effects on molecular electronic spectra. Frequency shifts. *J Phys Chem* 61:562–572

38. Krishnamoorthy G, Dogra SK (1999) Spectral characteristics of various prototropic species of 2-(4'-N, N-dimethylaminophenyl)pyrido[3,4-d]imidazole. *J Org Chem* 64:6566–6574
39. Dey JK, Dogra SK (1994) Dual fluorescence of 2-(4'-N, N-(dimethylamino) phenyl)benzothiazole and its imidazole analogue: effects of solvents and pH on electronic spectra. *J Phys Chem* 98: 3638–3644
40. Dash N, Chipem FAS, Krishnamoorthy G (2009) Encapsulation of 2-(4'-N, N-dimethylamino)-phenylimidazo[4,5-b]pyridine in β -cyclodextrin: effect on H-bond-induced intramolecular charge transfer emission. *Photochem Photobiol Sci* 8:1708–1715
41. Krishnamoorthy G, Dogra SK (1999) Dual fluorescence of 2-(4'-N-dimethylaminophenyl) imidazole: Effect of β -cyclodextrin and pH. *J Photochem Photobiol, A* 121:109–119